RAIN ESTIMATION OVER A REGION USING CYCLEGAN

Sergey Timinsky, Hai Victor Habi and Jonatan Ostrometzky

School of Electrical Engineering, Tel Aviv University, Israel

ABSTRACT

In the last couple of years, supervised machine learning (ML) methods have shown state-of-the-art results for near-ground rain estimation. Information is usually obtained from two kinds of sensors - rain gauges, which measure rain rate, and commercial microwave links (CMLs) which measure attenuation. These data sources are paired to create a dataset on which a model is trained. The arising problem of such methods of training is in the need for the datasets to be constructed with a CML-rain gauge pairing relation. In this paper, we propose a novel approach for rain estimation using a training method that does not require a matching between a CML and a rain gauge. Our goal is to infer the relation between CML measurements to rain rate values, with a data-driven approach using an unpaired dataset. We achieve this by inducing two cycle-consistency losses that capture the intuition that if we translate from attenuation measurements to rain rate observations and back again - we should arrive at where we started. Moreover, we learn two mapping functions translating between A (attenuation) and R (rain-rate), denoted by $G : \mathcal{A} \to \mathcal{R}$ and $F : \mathcal{R} \to \mathcal{A}$. No information is provided as to which sample in $\mathcal{A}$ matches which sample in $\mathcal{R}$. We demonstrate our results using estimated accumulated rain predictions and validate them with a nearby rain gauge station.

Index Terms— Commercial Microwave Links (CMLs), Rain Estimation, Generative Adversarial Networks, Cycle consistency

1 Introduction

Commercial microwave links (CMLs) offer a unique opportunity for the signal-processing community. Inferred signals provide an insightful view of the propagation of waves in the atmosphere. Depending on the widely distributed CMLs, it can provide alternative precipitation information with high spatial and temporal resolution as a complement to dedicated precipitation products. More than a decade ago, Messer et al. introduced the novel use of the *Power-Law* for retrieving the rain estimates from CML measurements using traditional signal processing methods [1]. Since then there has been a growing body of research on the subject (see [2–4] among many others). The main idea is based on the fact that by knowing the power-law relation between rain-induced attenuation and rain rate [5], the average rain rate throughout the CML path can be retrieved [6–10].

Recently, machine learning (ML) and specifically deep learning (DL) has shown state-of-the-art results in several precipitations-attenuation relations with methods such as support vector machine [11], convolutional neural networks [12] and long-short term memory neural networks [13, 14] along other methods [15, 16]. All have been applied for identifying and estimating precipitation with considerable accuracy. However, implementing ML models require adequate labeled data, and one of the significant limitations is the necessity of paired datasets, meaning that each CML should have a nearby rain gauge. If the matching is not explicitly specified, we call that an *unpaired* dataset.

In this work, we suggest a new training method for rain estimation using *unpaired* cyclic consistency [17]. This means that a model is trained to translate a source domain to a target domain in the absence of paired examples. We apply cyclic consistency to translate attenuation measurements to rain rate observations using unpaired measurements of CMLs attenuation and rain gauge observations. However, the rain-rate distribution is imbalanced [18], and we address this imbalance by modifying the cyclic consistency. Using this new approach, we train a rain estimation model using an unpaired dataset of CMLs attenuation measurements and rain gauge observations from the same region (an area of approximately 30 km^2). We perform an experiment using data from the Netherlands and present preliminary results of the suggested approach.

The contribution of this work includes[1]: i) We suggest a modified consistency loss which considers the imbalance distribution of rain rate; ii) We propose a new training method for rain estimation models with an unpaired dataset of CMLs attenuation measurements and rain gauge observations via cycle constancy; and iii) We demonstrate our method on data from the Netherlands and show competitive results with unpaired training methods.

The rest of this paper is organized as follows: In Section 2, we provide full details on the data set used in this study. In Section 3, we describe the training method and network architecture of the model. Section 4 describes the experiment's results and implications. Lastly, in Section 5, we discuss the limitations of the study and present our conclusions.

2 Data

In this work, we use a dataset that contains 29 CMLs and three rain gauges in the Netherlands. Figure 1 depicts a geographic region where a selected group of CMLs and rain gauges are situated. The rain rate dataset (i.e., the rain gauge observations) was provided by KNMI [19], whereas, for the attenuation measurements, we used the dataset detailed in [20].

Let x_T^{long} and x_T^{lat} be the transmitting longitude and latitude coordinates, respectively, and x_R^{long} and x_R^{lat} are the receiving longitude and latitude coordinates, respectively. Then, the metadata of j^{th} CML is given by:

$$\boldsymbol{x}^{(j)} = [x_T^{long}, x_T^{lat}, x_R^{long}, x_R^{lat}]. \tag{1}$$

The CMLs-based dataset consists of minimum and maximum received signal level (RSL) measurements collected by the CMLs hardware (one minimum and one maximum RSL values within 15-minute interval are reported for every such interval).[2] The rain rate observation were sampled every 15 minutes by rain gauges. All

[1]The code used in this paper is publicly available at: https://github.com/sagitiminsky/CDEM

[2]The minimum and maximum values of the transmitted signal level (TSL) were also collected, but assumed constant so were not included in the following.

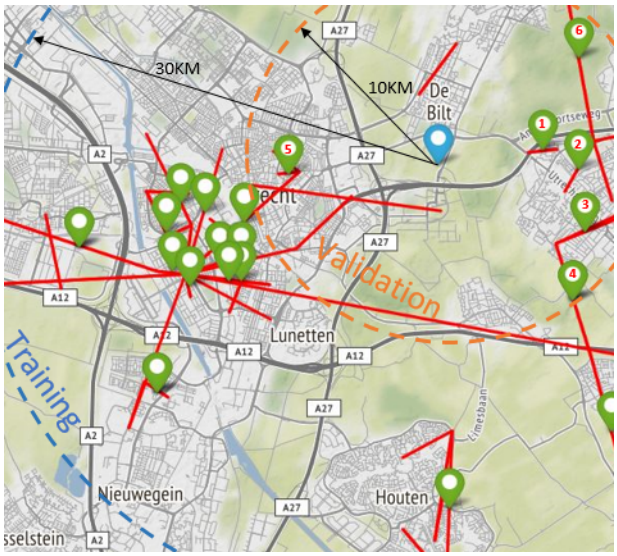

Fig. 1: Location of real CMLs [red], real rain gauges [blue], and inferring rain gauges [green] in the Netherlands during the training phase. We visualize inferring rain gauges only on the validation set. Notice that rain gauges 1-6 are in the radius of 1 km from a real rain gauge, which will serve as ground truth for the validation phase.

CMLs are in the same region as the rain gauges and all CMLs operate at the frequency range of 30 GHz - 45 GHz. In this work, we use n successive measurements as the input of our models.

The CML RSL measurements were pre-processed in a method inspired by the dynamic baseline evaluation process suggested in [21], to remove any long-term attenuation causing effects (such as free air propagation, and slow changing atmospheric phenomena as air pressure and humidity changes). Specifically, we calculated the minimal value inside a window size of 15 samples[3] around each of the received signal level (RSL) time series sampled, and subtracted these minimal values from the corresponding minimum and maximum RSL time-series values as follows:

$$\overline{MRSL_i} = MRSL_i - min(MRSL_{i-7}, ..., MRSL_{i+7}) \quad (2a)$$

$$\overline{mRSL_i} = mRSL_i - min(mRSL_{i-7}, ...mRSL_{i+7}) \quad (2b)$$

where $MRSL_i$ and $mRSL_i$ are the maximum and minimum RSL time-series values at time index i. Since the RSL measurements correspond to the attenuation values (up to a the constant TSL values), we used them directly to define the attenuation measurements matrix $\boldsymbol{X}_i^{(j)} \in \mathbb{R}^{2\times n}$ of the j^{th} CML and i^{th} time sample, which is a sequence of n consecutive measurements taken every 15 minutes:

$$\boldsymbol{X}_i^{(j)} = \begin{bmatrix} \overline{MRSL_i}, ..., \overline{MRSL_{(i+n)}} \\ \overline{mRSL_i}, ..., \overline{mRSL_{(i+n)}} \end{bmatrix}, \quad (3)$$

where $\overline{MRSL_i}$ and $\overline{mRSL_i}$ are the maximum and minimum RSL series after the removal of the other-than-rain attenuation factors. We normalize the attenuation measurements sequence to be in range between -1 and 1. The normalization is performed as follows: $\frac{\boldsymbol{X}_i^{(j)} - x_{min}}{x_{max} - x_{min}}$ where $x_{min} = \min_{i',j'} x_{i'}^{(j')}$ and $x_{max} = \max_{i',j'} x_{i'}^{(j')}$ are the minimal and maximal values which are calculated over all samples for all CMLs. We refer to this as the attenuation measurement sequence.

Next, we describe the rain rate which is measured via rain gauges. Specifically, the k^{th} rain rate time series of the measurements sampled every 15 minutes:

$$\boldsymbol{y}_i^{(k)} = \left[RR_i, ..., RR_{(i+n)}\right], \quad (4)$$

where RR_i to $RR_(i+n)$ are n measurement of rain rate. We apply the same normalization technique as we did for CMLs but with rain rate data. We normalize the rain rate sequence to be in the range between -1 and 1. Similarly: $\frac{\boldsymbol{y}_i^{(k)} - y_{min}}{y_{max} - y_{min}}$ where $y_{min} = \min_{i',k'} \boldsymbol{y}_{i'}^{(k')}$ and $y_{max} = \max_{i',k'} \boldsymbol{y}_{i'}^{(k')}$ are the minimal and maximal values which are calculated over all samples of all rain gauges. We refer to this as the rain rate observation sequence.

The rain-rate distribution is a well-studied subject [18,22] and it is shown that low rain rate have a higher probability. This poses a challenge to ML algorithms [23] since it produces imbalanced datasets. During the experiment time in the Netherlands, 95% of the time was dry whereas only in 5% of the time rain was observed, which illustrates the imbalance problem. We address this problem by adding a regularization which is presented in Section 3.1.

3 Method

In this section, we present our approach of regional training of rain estimation model using CycleGAN [17]. During training, we randomly select an unpaired sample of attenuation observation $\boldsymbol{X}_i^{(j)} \in \mathcal{A}$ and rain rate $\boldsymbol{y}_i^{(j)} \in \mathcal{R}$ from the same region where $\mathcal{A}$ is the attenuation domain and $\mathcal{R}$ is the rain-rate domain. By the same region, we mean that the CML and rain gauge are located in a similar meteorological area. In practice, we select a sample of attenuation measurements and rain rate observations produced by a CML and a rain gauge with a distance smaller than u = 30 km. Then, using those, we learn two mapping functions: 1) $G : \mathcal{A} \to \mathcal{R}$ is a function that maps attenuation measurements into rain rate observations; 2) $F : \mathcal{R} \to \mathcal{A}$ is a function that maps rain rate observations to attenuation measurements. To effectively learn G and F, we employ the idea of cycle consistency, meaning $F\left(G\left(\boldsymbol{X}_i^{(j)}\right)\right) \approx \boldsymbol{X}_i^{(j)}$ and $G\left(F\left(\boldsymbol{y}_i^{(j)}\right)\right) \approx \boldsymbol{y}_i^{(j)}$. Cycle consistency allows us to avoid directly comparing attenuation measurements and rain rate observations, eliminating the need for a paired dataset. In addition, to ensure that the G and F produce samples from $\mathcal{R}$ and $\mathcal{A}$ domains, respectively. We add two discriminators $D_R : \mathcal{R} \to (0, 1)$, $D_A : \mathcal{A} \to (0, 1)$ which enforce G and F to output samples that are from the two domains $\mathcal{R}$ and $\mathcal{A}$, respectively as in CycleGAN [17]. Each discriminator is trained to identify if a sample is "fake" or "real" and later is used to guide the generator to produce the samples from the correct domain. This results in a *min-max* optimization problem. At the end of the training, we take the generator G, which can map an attenuation measurement sequence to a rain rate observation sequence. In the sequel, we describe the loss function of our approach and the specific neural network architecture used in this work.

3.1 Region Learning via Cycle Consistency

Here, we describe the loss function used for regional learning via cycle consistency. We begin with adversarial Loss [24]. In adversarial training, a discriminator tries to distinguish between generated and real data. Then the generator tries to produce samples that fool

[3]The windows size of 15 samples used here is relatively long and was used to remove any other-than-rain constant or slow-changing attenuation-related phenomena.

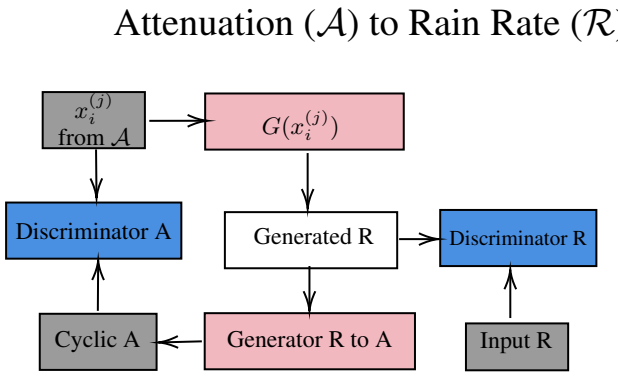

Fig. 2: The model operates across both attenuation and rain rate domains through the selection of a sample from each domain. Subsequently, the selected sample from the source domain is transformed into the destination domain by the generator. This newly generated sample is then passed to another generator, which converts it back into a cyclic sample. To ensure that the generated cyclic sample remains consistent with the original input sample, we enforce a condition of close similarity between the two. Meanwhile, the discriminator evaluates the similarity of the generated sample to the real sample and identifies samples generated by the adversary.

the discriminator. This results in the following *min-max optimization*:

$$\min_G \max_D \ell_{GAN}(G, D, \mathcal{A}, \mathcal{R}), \tag{5}$$

where

$$\begin{aligned}\ell_{GAN}(G, D, \mathcal{A}, \mathcal{R}) = \mathbb{E}_{y\in\mathcal{R}} \log D(y) \\ + \mathbb{E}_{x\in\mathcal{A}} \log(1 - D(G(x)),\end{aligned} \tag{6}$$

is the adversarial loss term. The generator must be able to fool the discriminator about the authenticity of its generated samples. Since we have two domains with corresponding generators G, F and discriminators D_R, D_A. Thus we employ the adversarial loss twice: $\ell_{GAN}(G, D_R, \mathcal{A}, \mathcal{R})$ and $\ell_{GAN}(F, D_A, \mathcal{R}, \mathcal{A})$ once per generator and it's discriminator.

Now, we describe the cycle consistency loss, which forms the fundamental concept that facilitates regional training. The cycle consistency enforces the models G and F to translate a sample from one domain to a different domain and back to the original one, namely $F\left(G\left(\boldsymbol{X}_i^{(j)}\right)\right) \approx \boldsymbol{X}_i^{(j)}$ and $G\left(F\left(\boldsymbol{y}_i^{(j)}\right)\right) \approx \boldsymbol{y}_i^{(j)}$. For example, in our case, we take a rain-rate sequence and map it into an attenuation measurement sequence. Then, the cycle consistency ensures that the attenuation measurements sequence can be mapped back to the *same* rain-rate sequence. Nonetheless, the utilization of rain estimation dataset presents an inherent imbalance, as detailed in Section 2. To address this issue, we propose adjusting the loss by the complementary distribution. Various types of well-known distributions can be utilized to model the rain rate distribution. In this work, we use the exponential distribution (7) as a model of rain rate observations and attenuation measurements distributions [18]:

$$f(r) = \beta \mathrm{e}^{-\beta r} \qquad \forall r \geq 0, \tag{7}$$

where β is the exponential distribution parameter. We fit the parameter β_A and β_B of the exponential distribution using least squares on a collection of rain rates and dynamic baseline evaluations of the attenuation measurements [18]. Specifically, we minimize the modified cycle consistency [17] loss which is defined as:

$$\min_{G,F} \ell_{cyc}(G, F), \tag{8}$$

where

$$\begin{aligned}\ell_{cyc}(G, F) \triangleq \mathbb{E}_{x\in\mathcal{A}}((\alpha + 1 - f(x; \beta_A))||F(G(x)) - x||_1) \\ + \mathbb{E}_{y\in\mathcal{R}}((\alpha + 1 - f(y; \beta_R))||G(F(y)) - y||_1).\end{aligned} \tag{9}$$

is the cycle consistency loss and $||a||_1$ denote the ℓ_1 norm of vector a. The term α ensures that the expectations do not become null. Notice that ℓ_{cyc} addresses the imbalanced datasets problem for the rain estimation problems by introducing two regularization terms: $f_{RR}(x; \beta_A))$ and $f_{RR}(y; \beta_R))$ which push G towards higher rain rates values. Finally, we combine the adversarial loss, cycle consistency loss and the rain distribution regularization into a single optimizing problem:

$$\min_{G,F} \max_{D_\mathcal{R}, D_\mathcal{A}} \ell(G, F, \mathcal{A}, \mathcal{R}), \tag{10}$$

where

$$\begin{aligned}\ell(G, F, \mathcal{A}, \mathcal{R}) = \ell_{GAN}(G, D_\mathcal{R}, \mathcal{A}, \mathcal{R}) \\ + \ell_{GAN}(F, D_\mathcal{A}, \mathcal{A}, \mathcal{R}) \\ + \lambda \ell_{cyc}(G, F)\end{aligned} \tag{11}$$

is the combined loss function, and λ is a hyper-parameter that controls the effect of cycle consistency loss.

3.2 Network

In this section, we described the specific implementation of the mapping G, F and the discriminators D_R, D_A. We use a convolution neural network to implement G, F, D_R and D_A. We begin with the description of generator G and F. The generators are built as follows: starting with three convolution layers followed by three residual blocks [25]. In the last part of the generators, there are three transpose convolution layers [26]. After each convolution and transpose convolution, we add a batch-normalization layer [27] followed by a ReLu non-linear function. In the last generator layer we use a *tanh* activation function. An illustration of the generator structure is presented in Figure 3.a.

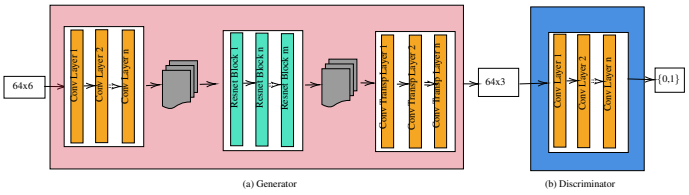

Fig. 3: (a) The pink-colored component is tasked with generating the rain rate observations based on attenuation measurements. The counterpart generator that produces the attenuation measurements from rain rate observations shares similarities with its counterpart, except for the input and output sizes, which alternate between 64×6 and 64×3. (b) The rain rate discriminator is marked in blue. The attenuation discriminator employs identical components, with an input shape of 64×6.

The discriminator has a simpler network structure with three convolution layers. Batch normalization and *ReLu* non-linear functions are added after each convolution layer, similar to the generator. Figure 3.b. shows an illustration of the discriminator structure.

4 Experiment and Results

The dataset was split into 20 CMLs and two rain gauges for training and nine CMLs, and one rain gauge for validation as shown in Figure 1. Training took place on June 9th-11th and August 5th-8th, 2011, over seven days, with validation performed on August 5th-8th, 2011. Multiple rain events were considered, and the performance of inferring rain rate from a set of CMLs in a given region was evaluated using the root-mean-squared-selective-error (RMSSE) [28] metric between the closest gauge x and CML y during validation. We defined u=10 km as the distance between a CML and a rain gauge in the validation set. For the training dataset, any two pairs could be chosen in the region of u = 30 km. The RMSSE metric for validation is defined as follows:

$$\text{RMSSE}_j = \sqrt{\frac{1}{N}\sum_{\substack{i\in\mathcal{I}_j \\ p}}\left(G\left(\boldsymbol{X}_i^{(j)}\right)_p - y_{i,p}^{(k(j))}\right)^2},$$

where $k(j)$ is the index of the closest rain gauge to j^{th} CML and $\mathcal{I}_j$ is the set of indexes on which the RMSSE is computed. The set $\mathcal{I}_j = \{(i,p) : y_{i,p}^{(k(j))} > 1 || G\left(\boldsymbol{X}_i^{(j)}\right)_p > 0.5\}$ used for calculating the RMSSE for high-intensity rain events with actual rain rates greater than 1 mm/h and predicted rain rates higher than 0.5 mm/h. p denotes the p element of the vector.

The network had three hidden layers, with 64 filters in the generator/discriminator's last/first layer. Adam [29] optimization was used for stochastic gradient descent. A learning rate of 0.0002 with a linear decay every 50 epochs, batch size 1, and no dropout were used. The selected GPU instance was NVIDIA T4. $\lambda = 10$ was used for the cyclic loss, indicating that it was given 10 times more importance than GAN loss. We set n = 64 for (3) and (4) and $\alpha = 0.2$ for (9). The RMSSE values were calculated for high-intensity rain events only, meaning that we included real rain rate events higher than 1 mm/h and predicted rain rate higher than 0.5 mm/h. The values of the six validation stations are presented in Figure 4.

Table 1: Steady state metrics of training and validation

	Training	**Validation**
$G_{\mathcal{A}to\mathcal{R}}$	0.3189	0.3203
$G_{\mathcal{R}to\mathcal{A}}$	0.8122	0.8122
$D_{\mathcal{R}}$	0.2396	0.1042
$D_{\mathcal{A}}$	0.5092	0.5054
$Cycle_{\mathcal{A}}$	0.1196	0.2036
$Cycle_{\mathcal{R}}$	0.02355	0.02355

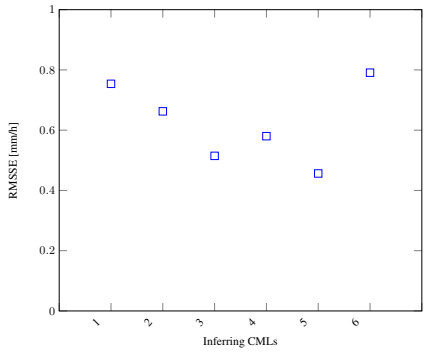

Fig. 4: RMSSE values of six inferring CMLs in within a 10 km radius of a nearby rain gauge (marked as orange circle in Figure 1) for the the validation iteration.

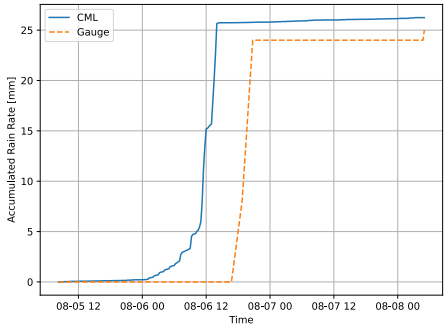

Fig. 5: Predicted accumulated rain rate [blue] vs ground truth accumulated rain rate [orange] for CML #6.

The RMSSE values are low, indicating that the generated attenuation measurements from the CML sequence are close to the ground truth rain rate observations sequence for all stations in the validation set.

5 Conclusion & Future work

In this study, we make use of an unpaired dataset of CML-based attenuation measurements and rain gauge observations to train a rain estimation model. Cycle consistency between attenuation and rain-rate domains is used instead of a direct match between specific CML and rain gauge. The modified cycle consistency accounts for rain rate imbalance. Experimental results from the Netherlands are presented and are encouraging. However, there are still unanswered questions about the necessary amount of rain gauges and CMLs for a correct and accurate model, the training region size, and obtaining cycle consistency between CML and an entire rain field covering a selected area of interest.

Acknowledgement

We are grateful to Dr. Aart Overeem and the Royal Netherlands Meteorological Institute (KNMI) for providing the rainfall dataset and CMLs data used in this work. We would like also to thank Prof. Hagit Messer, Prof. Pinhas Alpert, and the entire CellEnMon Lab team at Tel Aviv University.

References

[1] H. Messer, A. Zinevich, and P. Alpert, "Environmental monitoring by wireless communication networks," *Science*, vol. 312, no. 5774, pp. 713–713, 2006.

[2] R. Uijlenhoet, A. Overeem, and H. Leijnse, "Opportunistic remote sensing of rainfall using microwave links from cellular communication networks," *Wiley Interdisciplinary Reviews: Water*, vol. 5, no. 4, p. e1289, 2018.

[3] C. Chwala and H. Kunstmann, "Commercial microwave link networks for rainfall observation: Assessment of the current status and future challenges," *Wiley Interdisciplinary Reviews: Water*, vol. 6, no. 2, p. e1337, 2019.

[4] D. Cherkassky, J. Ostrometzky, and H. Messer, "Precipitation classification using measurements from commercial microwave links," *IEEE Transactions on Geoscience and Remote Sensing*, vol. 52, no. 5, pp. 2350–2356, 2013.

[5] R. Olsen, D. V. Rogers, and D. Hodge, "The ar b relation in the calculation of rain attenuation," *IEEE Transactions on antennas and propagation*, vol. 26, no. 2, pp. 318–329, 1978.

[6] F. Saggese, V. Lottici, and F. Giannetti, "Rainfall map from attenuation data fusion of satellite broadcast and commercial microwave links," *Sensors*, vol. 22, no. 18, p. 7019, 2022.

[7] M. Graf, A. El Hachem, M. Eisele, J. Seidel, C. Chwala, H. Kunstmann, and A. Bárdossy, "Rainfall estimates from opportunistic sensors in germany across spatio-temporal scales," *Journal of Hydrology: Regional Studies*, vol. 37, p. 100883, 2021.

[8] A. Eshel, P. Alpert, and H. Messer, "Estimating the parameters of the spatial autocorrelation of rainfall fields by measurements from commercial microwave links," *IEEE Transactions on Geoscience and Remote Sensing*, vol. 60, pp. 1–11, 2022.

[9] Y. Zhao, X. Liu, K. Pu, J. Ye, and M. Xian, "Research on the method of rainfall field retrieval based on the combination of earth–space links and horizontal microwave links," *Remote Sensing*, vol. 14, no. 9, p. 2220, 2022.

[10] A. Overeem, H. Leijnse, T. C. van Leth, L. Bogerd, J. Priebe, D. Tricarico, A. Droste, and R. Uijlenhoet, "Tropical rainfall monitoring with commercial microwave links in sri lanka," *Environmental Research Letters*, vol. 16, no. 7, p. 074058, 2021.

[11] K. Song, X. Liu, M. Zou, D. Zhou, H. Wu, and F. Ji, "Experimental study of detecting rainfall using microwave links: Classification of wet and dry periods," *IEEE Journal of Selected Topics in Applied Earth Observations and Remote Sensing*, vol. 13, pp. 5264–5271, 2020.

[12] J. Polz, C. Chwala, M. Graf, and H. Kunstmann, "Rain event detection in commercial microwave link attenuation data using convolutional neural networks," 2020.

[13] H. V. Habi and H. Messer, "Recurrent neural network for rain estimation using commercial microwave links," *IEEE Transactions on Geoscience and Remote Sensing*, vol. 59, no. 5, pp. 3672–3681, 2020.

[14] B. He, X. Liu, S. Hu, K. Song, and T. Gao, "Use of the c-band microwave link to distinguish between rainy and dry periods," *Advances in Meteorology*, vol. 2019, 2019.

[15] H. V. Habi and H. Messer, "Uncertainties in short commercial microwave links fading due to rain," in *ICASSP 2020-2020 IEEE International Conference on Acoustics, Speech and Signal Processing (ICASSP)*, pp. 9006–9010, IEEE, 2020.

[16] J. Pudashine, A. Guyot, F. Petitjean, V. R. Pauwels, R. Uijlenhoet, A. Seed, M. Prakash, and J. P. Walker, "Deep learning for an improved prediction of rainfall retrievals from commercial microwave links," *Water Resources Research*, vol. 56, no. 7, p. e2019WR026255, 2020.

[17] J.-Y. Zhu, T. Park, P. Isola, and A. A. Efros, "Unpaired image-to-image translation using cycle-consistent adversarial networks," in *Proceedings of the IEEE international conference on computer vision*, pp. 2223–2232, 2017.

[18] D. Salisu, S. Supiah, A. Azmi, *et al.*, "Modeling the distribution of rainfall intensity using hourly data.," *American Journal of Environmental Sciences*, vol. 6, no. 3, pp. 238–243, 2010.

[19] I. Lütkebohle, "Hourly data of the weather in the Netherlands ." https://www.knmi.nl/nederland-nu/klimatologie/uurgegevens, 2008. [Online; accessed 24-December-2022].

[20] A. Overeem, "Overeem, Aart (2019): Commercial microwave link data for rainfall monitoring ." https://data.4tu.nl/articles/dataset/Commercial_microwave_link_data_for_rainfall_monitoring/12688253, 2019.

[21] J. Ostrometzky and H. Messer, "Dynamic determination of the baseline level in microwave links for rain monitoring from minimum attenuation values," *IEEE Journal of Selected Topics in Applied Earth Observations and Remote Sensing*, vol. 11, no. 1, pp. 24–33, 2017.

[22] F. Moupfouma, "Model of rainfall-rate distribution for radio system design," in *IEE Proceedings H (Microwaves, Antennas and Propagation)*, vol. 132, pp. 39–43, IET, 1985.

[23] H. V. Habi, "Rain detection and estimation using recurrent neural network and commercial microwave links," *M. Sc. Thesis*, 2019.

[24] J. Ian, "Goodfellow, jean pouget-abadie, mehdi mirza, bing xu, david warde-farley, sherjil ozair, aaron courville, yoshua bengio. generative adversarial networks," *Advances in Neural Information Processing Systems*, vol. 27, pp. 8–13, 2014.

[25] K. He, X. Zhang, S. Ren, and J. Sun, "Deep residual learning for image recognition," in *Proceedings of the IEEE conference on computer vision and pattern recognition*, pp. 770–778, 2016.

[26] V. Dumoulin and F. Visin, "A guide to convolution arithmetic for deep learning," *arXiv preprint arXiv:1603.07285*, 2016.

[27] S. Ioffe and C. Szegedy, "Batch normalization: Accelerating deep network training by reducing internal covariate shift," in *International conference on machine learning*, pp. 448–456, pmlr, 2015.

[28] T. Weiss, T. Routtenberg, and H. Messer, "Total performance evaluation of intensity estimation after detection," *Signal Processing*, vol. 183, p. 108042, 2021.

[29] D. P. Kingma and J. Ba, "Adam: A method for stochastic optimization," *arXiv preprint arXiv:1412.6980*, 2014.